



**HAL**  
open science

## Synthesis and characterization of new hybrid decatungstate anions (CTAB)<sub>4</sub>W<sub>10</sub>O<sub>32</sub>: Toward heterogeneous Photocatalysis

Samir Briche, El Mountassir El Mouchtari, Mustapha Boutamart, Oussama Jhabli, Lekbira El Mersly, Kaltoum Belkodia, Mohammed Amine Edaala, Pascal Wong-Wah-Chung, Otman Abida, Salah Rafqah

### ► To cite this version:

Samir Briche, El Mountassir El Mouchtari, Mustapha Boutamart, Oussama Jhabli, Lekbira El Mersly, et al.. Synthesis and characterization of new hybrid decatungstate anions (CTAB)<sub>4</sub>W<sub>10</sub>O<sub>32</sub>: Toward heterogeneous Photocatalysis. International Journal of Environmental Analytical Chemistry, In press, 10.1080/03067319.2023.2242267 . hal-04435878

HAL Id: hal-04435878

<https://hal.science/hal-04435878v1>

Submitted on 6 Feb 2024

**HAL** is a multi-disciplinary open access archive for the deposit and dissemination of scientific research documents, whether they are published or not. The documents may come from teaching and research institutions in France or abroad, or from public or private research centers.

L'archive ouverte pluridisciplinaire **HAL**, est destinée au dépôt et à la diffusion de documents scientifiques de niveau recherche, publiés ou non, émanant des établissements d'enseignement et de recherche français ou étrangers, des laboratoires publics ou privés.



Distributed under a Creative Commons Attribution - NonCommercial - NoDerivatives 4.0 International License

# Synthesis and characterization of new hybrid decatungstate anions (CTAB)<sub>4</sub>W<sub>10</sub>O<sub>32</sub> : Toward heterogeneous Photocatalysis

Samir Briche<sup>a</sup>, El mountassir El mouchtari<sup>b,c</sup>, Mustapha Boutamart<sup>a</sup>, Oussama Jhabli<sup>a</sup>,  
Lekbira El Mersly<sup>b</sup>, Kaltoum Belkodia<sup>b</sup>, Mohammed Amine Edaala<sup>b</sup>, Pascal Wong-Wah-  
Chung<sup>c</sup>, Otman Abida<sup>d</sup>, Salah Rafqah<sup>b</sup>.

<sup>a</sup> Department of Energy Storage and Multifunctional Coatings, Moroccan Foundation for Advanced Science, Innovation and Research (MAScIR), Rabat, Morocco.

<sup>b</sup> Laboratoire de Chimie Analytique et Moléculaire, Faculté polydisciplinaire de Safi, Université Cadi Ayyad, Morocco.

<sup>c</sup> Aix Marseille Université, CNRS, LCE, Marseille, France

<sup>d</sup> College of Engineering, American University of the Middle East, Egaila, Kuwait.

## Abstract:

In the present study, hybrid decatungstate based photocatalysts, [(C<sub>16</sub>H<sub>33</sub>)N(CH<sub>3</sub>)<sub>3</sub>]<sub>4</sub>[W<sub>10</sub>O<sub>32</sub>], were synthesized by the reaction of hexadecyltrimethylammonium surfactant (CTAB) and Na<sub>4</sub>W<sub>10</sub>O<sub>32</sub>.2.6H<sub>2</sub>O (W10), with different molar ratio W10:CTAB (1:1 for compound 1 and 1:3 for compound 2). In order to verify that the materials have been formed, FTIR, UV-visible spectroscopy, TGA, XRD, and SEM tests were conducted. Comparing and analyzing the influences of molar ratios on band gap energy, photocatalytic activity, and material morphology is discussed. FTIR spectroscopy showed that CTAB reacted with W10 to produce an insoluble product in aqueous media. According to UV-visible spectroscopy, the hybrid material with a low amount of CTAB absorbs more light in the visible region than the other, with the optical band gap decreasing to 2.42 eV for compound 1. After 7 hours of exposure, both compounds, compound 1 and 2, demonstrated a 46 and 88% degradation of carbamazepine in aqueous solution using UV-visible photocatalysis.

**Keywords:** Hybrid decatungstate, heterogeneous photocatalysis, carbamazepine, water purification.

## 1. Introduction

Polyoxometalates (POMs) are metal-oxide species built from pseudo-octahedral MO<sub>6</sub> (M=V, Nb, Mo, W) units sharing corners and/or edge with the metal is in its higher oxidation degree.

35 Recently, POMs attracted a lot of attention for their promising proprieties in many application  
36 fields: catalysis and photocatalysis [1–6], biology [7] and medicine [8]. The POMs showed  
37 good redox reversibility, producing colored mixed-valence species while maintaining their  
38 structural integrity [9]. Among these POMs is decatungstate ion  $W_{10}O_{32}^{4-}$ , which is an  
39 isopolytungstate with a metal-oxide framework without any internal heteroatoms or heteroions.  
40 It has been widely used as a homogenous photocatalysts [10–12] for organic reactions and  
41 organic pollutant degradation in water [10,13–15], because of its interesting physical properties  
42 such as, high surface charge density and strongly basic oxygen surfaces. Otherwise, the research  
43 on isopolyacids is still limited, while most of the research papers in POMs area are focused on  
44 the heteropolyacids [16–18].

45 Research efforts have been concentrated on wastewater treatment using PMOs through  
46 advanced oxidation processes over the past few years. These materials can be used to replace  
47 conventional semi-conductors photocatalysts, which suffer from photo-corrosion and limited  
48 visible light absorption [19]. Moreover, in decatungstate system, the reactive species has a quite  
49 long lifetime ( $\tau_{wO}$  of  $65 \pm 5$  ns) [20] and are formed with a high quantum yield ( $\Phi_{wO}$  is 0.57).  
50 Nevertheless, decatungstate is highly soluble in aqueous solutions, which limits their potential  
51 application in heterogeneous photocatalysis, and consequently, heterogenization of  
52 decatungstate remains an appealing challenge for researchers. There are various strategies to  
53 incorporate decatungstate in solid support materials among them  $SiO_2$ [21–25],  $ZrO_2$ [26,27],  
54  $TiO_2$ [28] and  $\gamma-Al_2O_3$ [29]. However, these composites revealed to be instable under irradiation  
55 and their activity limited due to the release of photoactive species in solution. Considering the  
56 very high photoactivity of decatungstate [30] it appeared sometimes difficult to attribute the  
57 observed efficiency to the heterogenous or homogeneous photocatalysis phenomenon. As  
58 result, solubility control was shown to be a key aspect of POM chemistry and application. The  
59 use of organic surfactant as hexadecyltrimethylammonium (CTAB) for POMs heterogenization  
60 was recently reported [31], and the hybrid materials obtained were structurally characterized  
61 without any application studies [32–34]. The CTAB cationic surfactant is very in water and  
62 environmentally friendly compounds, making it an ideal candidate for decatungstate  
63 heterogenization.

64 The aim of this work is to synthesize new water-insoluble heterogeneous decatungstate based  
65 photocatalysts, determine their structural properties and assess their photocatalytic activity  
66 through pollutant degradation. Carbamazepine (CBZ) was chosen as a pharmaceutical pollutant  
67 model for two reasons: (i) the use of classical dyes that are inappropriate for photocatalytic  
68 activity studies under visible light [35,36] (ii) CBZ in one of the most common pollutant

69 detected in wastewater and its elimination has been extensively studied [37–41], (iii) CBZ is  
70 almost photostable under visible light irradiation. Considering that the leaching of  
71 decatungstate is also one of our main concerns, we focused on a simple test that could be used  
72 as a standard one to test for hybrid materials based on decatungstate.

## 73 **2. Experimental section**

### 74 **2.1. Materials and Methods**

#### 75 **2.1.1. Chemicals**

76 All Chemical reagents, hydrochloric acid (HCl; 37% purity), sodium chloride (NaCl; 99%  
77 purity), acetonitrile (CH<sub>3</sub>CN; 99.5% purity) and Hexadecyltrimethylammonium bromide  
78 (CTAB, 96% purity) were purchased from Sigma-Aldrich except sodium tungstate dihydrate  
79 (Na<sub>2</sub>WO<sub>4</sub>·2H<sub>2</sub>O, 99% purity) purchased from CARLO ERBA. All chemicals were used without  
80 further purification.

#### 81 **2.1.2. Characterization equipment**

82 FTIR spectra were acquired in transmission mode in the 4000–400 cm<sup>-1</sup> spectral range using an  
83 ABB Bomem FTLA200 spectrometer and KBr pellet technique. Spectra of 16 scans were  
84 recorded in air atmosphere with a resolution of 16 cm<sup>-1</sup>. Thermogravimetric analysis (TGA)  
85 was performed under air atmosphere using TGA Q500 (TA 1000) equipment. The specimens  
86 (approximately 20 mg) were weight in Platinum crucible. The samples were heated at a rate of  
87 5°C.min<sup>-1</sup> from ambient temperature to 1000°C. The powder XRD data were collected on a  
88 Philips diffractometer, using Cu K $\alpha$  radiation from 5° to 80° (2 $\theta$ ) with 0.02° step. The UV-  
89 visible solid-state absorption spectra were recorded from a sample powder in quartz cell 1 mm-  
90 diameter on a Perkin Elmer Lambda 1050 UV/Visible/NIR instrument from 200 to 800 nm with  
91 1 nm step and a 150 InGaAs mm-diameter integrating sphere. The surface morphology of  
92 materials was analysed using High-resolution Scanning Electron Microscopy (SEM) with  
93 BRUKER-QUANTAX FEI instrument operated at 200 keV.

#### 94 **2.1.3. Photocatalytic experiments**

95 The experiments were conducted with a LOT Quantum Xenon Lamp system (300 W) equipped  
96 with a 90° beam turner whose emission was filtered by a water and atmospheric filter (LOT  
97 Quantum Design LSZ231 and LSZ176) to deliver a wavelength ranged between 290-800 nm.  
98 A photocatalyst sample of 30 mg was suspended in 50 mL of an aqueous solution of  
99 Carbamazepine (CBZ) at 1×10<sup>-4</sup> mol.L<sup>-1</sup>. After 1 hour stirring in the dark at room temperature  
100 (25°C), the adsorption/desorption equilibrium was reached. The mixture was then placed in a

101 reactor (pyrex glass), and continuously stirred throughout the experiment. Mixture and reactor  
102 were kept at 20 °C by water flow [41].

#### 103 **2.1.4. HPLC and LC MS analysis of CBZ**

104 The concentration of **CBZ** was determined by liquid chromatography apparatus (UPLC  
105 PerkinElmer Altus 30) equipped with an Eclipse Plus C18 (3.5 µm; 2.5 × 150 mm) and a  
106 220/240 pump, a 330-diode array UV-visible detector, a 363-fluorescence detector and a 410-  
107 automatic injector. An isocratic method was set at a flow rate of 0.25 mL.min<sup>-1</sup> and the injected  
108 volume was equal to 10 µL. The separation was obtained using a 65:35 ratio of  
109 water/acetonitrile (with 0.1% formic acid) and the wavelength of absorption used for detection  
110 was 285 nm. Before injection, samples were systematically filtered on a 0.2 µm cellulosic filter  
111 of 15 mm in diameter (Agilent Technologies) to remove the photocatalyst ensuring that CBZ  
112 was not retained on the filter.

113 Identification of carbamazepine degradation products was performed (LC-MS QTOF), using  
114 Agilent 1290. The source parameters were established as follows: fragmenter: 140 V, capillary  
115 voltage: 3000 V, skimmer 65 V, nebulizer pressure (30 psi), nebulizer needle voltage (500 V),  
116 nitrogen was used as desolvation gas (temperature 350°C, flow rate 10 L.min<sup>-1</sup>), and the flow  
117 rates for the sheath gas were set at 350°C and 8 L.min<sup>-1</sup> respectively.

### 118 **2.2.Synthesis of materials**

#### 119 **2.2.1. Synthesis of Na<sub>4</sub>W<sub>10</sub>O<sub>32</sub>. xH<sub>2</sub>O**

120 Na<sub>4</sub>W<sub>10</sub>O<sub>32</sub>.xH<sub>2</sub>O (**W10**) was prepared following literature procedures [42] with large  
121 modifications. First, a boiled aqueous solution of Na<sub>2</sub>WO<sub>4</sub>.2H<sub>2</sub>O (66 g in 400 mL) and HCl (1  
122 M in 400 mL) were mixed for 20 seconds under strong stirring, then the mixture was cooled  
123 rapidly to 0°C. When the temperature has reached 30°C, an excess of NaCl salt was added to  
124 the mixture and at 0°C, a precipitate was formed. This precipitate was filtered and dried in  
125 vacuum and about 33 g of light-yellow solid were collected and placed for one night in freezer  
126 at -3°C. After dissolving the solid in hot acetonitrile (200 mL for 33 g of the solid formed), the  
127 solution was boiled for 2 to 3 minutes, and filtering was performed. A white solid residue  
128 containing predominantly sodium chloride was collected and the yellow-green solution (the  
129 filtrate) was evaporated at 25°C to obtain a yellow-green powder.

130 **2.2.2. Synthesis of [(C<sub>16</sub>H<sub>33</sub>)N(CH<sub>3</sub>)<sub>3</sub>]<sub>4</sub>[W<sub>10</sub>O<sub>32</sub>] hybrid materials.** A 20 mL of aqueous  
131 solution of decatungstate **W10** (2.44 g, 1 mmol) was added dropwise to 20 mL of aqueous  
132 solution of **CTAB** at different concentration (0.36 g (1 mmol) for **compound 1** and 1.08 g (3  
133 mmol) for **compound 2**) under vigorous stirring. The mixture was refluxed at 100°C for 1 hour.

134 A pale-yellow precipitate was obtained for **compound 1**, and a white precipitate for **compound**  
135 **2**. The precipitates were washed and filtered three-times with hot water and then dried overnight  
136 at 100°C.

137

138

### 139 **3. Results and discussion**

#### 140 **3.1. Materials Characterization**

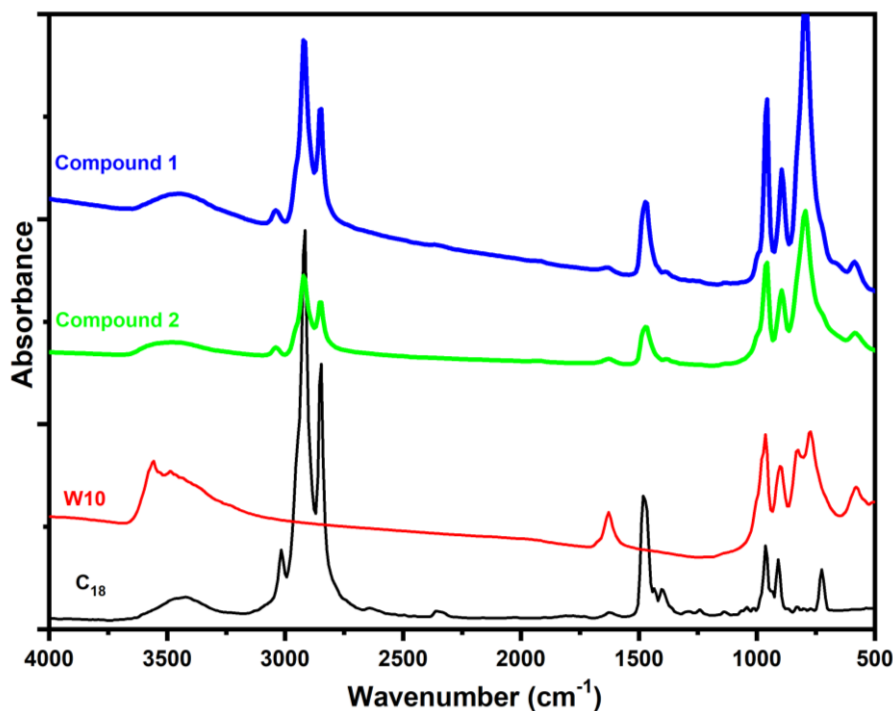
141 To further establish the formation of hybrid materials, FT-IR spectral measurements were  
142 carried out. The representative results are shown in Figure 1. The FT-IR spectrum of **W10**  
143 shows the well-known absorptions bands of decatungstate [43,44]. The absorption band at  
144 424.3  $\text{cm}^{-1}$  is assigned to W-O-W scissoring, the others at 578.6, 771.47, 833.18 and 902.62  
145  $\text{cm}^{-1}$  are assigned to W-O<sub>corner-shard</sub>-W and W-O<sub>edge-shard</sub>-W stretching in the decatungstate  
146 framework, and the intense band at 964.33  $\text{cm}^{-1}$  is assigned to the stretching of W=O<sub>terminal</sub>  
147 [42,45–47]. Two bands are well resolved for the bending vibrations of water. The highest  
148 frequency band in the  $\delta(\text{HOH})$  vibrations range, at 1658  $\text{cm}^{-1}$ , corresponds to the weakly bonded  
149 waters, however the band at 1627  $\text{cm}^{-1}$  belongs to coordinated water molecules but with a  
150 weaker coordination bond [48]. A band was observed within 3500  $\text{cm}^{-1}$  for stretching vibrations  
151 of water  $\nu(\text{OH})$ , corresponding to coordinated water molecules. We carried out a  
152 thermogravimetric analysis to determine how many water molecules were chemisorbed and  
153 physisorbed. Thus, we counted about 2.6 structural water molecules in each cluster.

154 On the FT-IR spectrum of CTAB molecule the strong absorption at 2847, 2916 and 3016  $\text{cm}^{-1}$   
155 respectively originated from C–H stretching vibration of methyl and methylene groups of  
156 CTAB. The absorption bands at 1481 and 1434  $\text{cm}^{-1}$  for pure hexadecyltrimethylammonium  
157 surfactant were due to the asymmetric and symmetric –C–H vibration of the quaternary  
158 ammonium group [44,49–51].

159 The FT-IR spectra of compounds **1** and **2** are similar with the characteristic's absorption bands  
160 of W10 and CTAB. This confirms that CTAB have successfully reacted with W10. The  
161 compounds **1** and **2** also bear the symmetric and asymmetric  $-(\text{CH}_2)-$  vibrations, which  
162 indicates the direct non-involvement of hydrocarbon chains in the reaction leading to the  
163 formation of compounds **1** and **2**. Additionally, the band at 1481  $\text{cm}^{-1}$  was broadened and  
164 shifted to 1465  $\text{cm}^{-1}$  and the peak at 1434  $\text{cm}^{-1}$  was not present, which suggest that hybrid  
165 materials influenced the quaternary ammonium group vibrations. In the stretching vibration

166 region at  $3448\text{ cm}^{-1}$ , a broad and less intense band was observed. This corresponds to adsorbed  
167 water molecules [52].

168



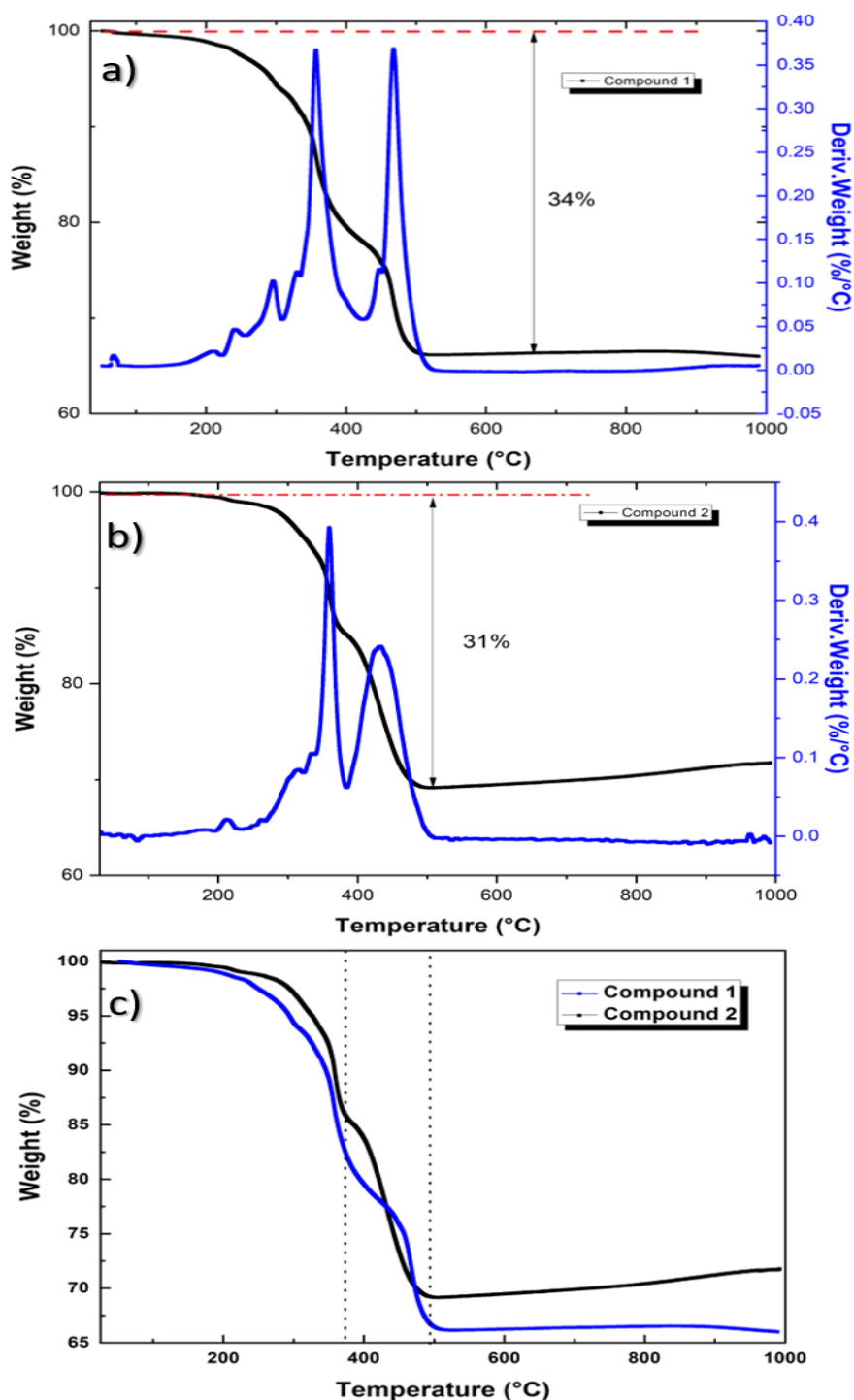
169

170 **Figure 1:** FT-IR spectra of W10, CTAB and hybrid materials (compound 1 and 2).

171

172 To investigate the thermal stability and establishing the chemical formula of compound **1** and  
173 **2**, a series of TGA experiments were carried out. The thermogravimetric analysis (figure 2),  
174 reveals that both compounds have almost similar thermal behaviour. Two main steps are  
175 observed in TGA for the decomposition process under air atmosphere. A first step ends at  
176 approximately  $375\text{ }^{\circ}\text{C}$ , and the second step is completed at approximately at  $500^{\circ}\text{C}$ . This  
177 represents a total weight loss of 34 and 31% for compound **1** and **2** respectively, which  
178 corresponds to the loss of 4 CTAB molecules.

179



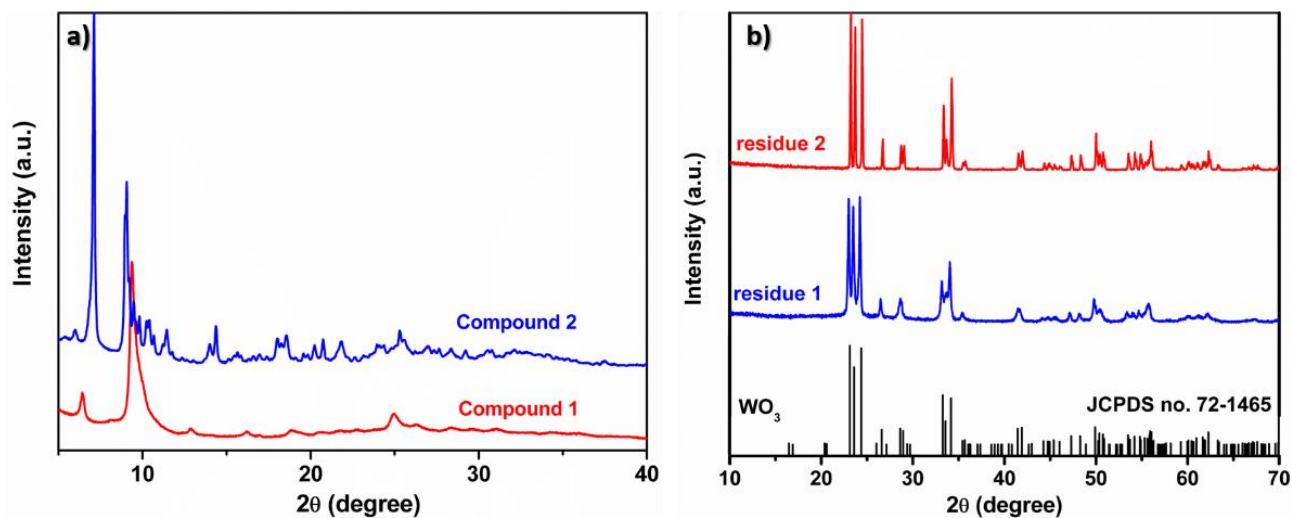
180

181 **Figure 2:** TGA curves of compound 1 (a) and compound 2 (b) and comparative curves (c).

182 Additionally, compound 2 decomposes at almost 50°C higher than the compound 1, which is a  
 183 reliable indicator of its stability. The relatively high thermal stability of compound 2 ought to  
 184 be attributed to the high crystallinity in comparison with compound 1 which is confirmed by  
 185 XRD analysis in figure 3a. On the other hand, this temperature shift might be also due to  
 186 encapsulation of CTAB ions, or strong interaction between CTAB and W10 [53,54]. In  
 187 addition, it is important to note that the powder diffraction pattern (figure 3b) collected from a



188 solid's residue after TGA experiments for both compounds, confirms the formation of tungsten  
 189 trioxide (WO<sub>3</sub>). Assuming the decomposition reaction (Eq.1), it can be shown that the observed  
 190 weight loss nearly precisely corresponds to x:y ratio 4:10. Thus, the chemical composition of  
 191 both compounds is (C<sub>19</sub>H<sub>42</sub>N)<sub>4</sub>W<sub>10</sub>O<sub>32</sub>.



193

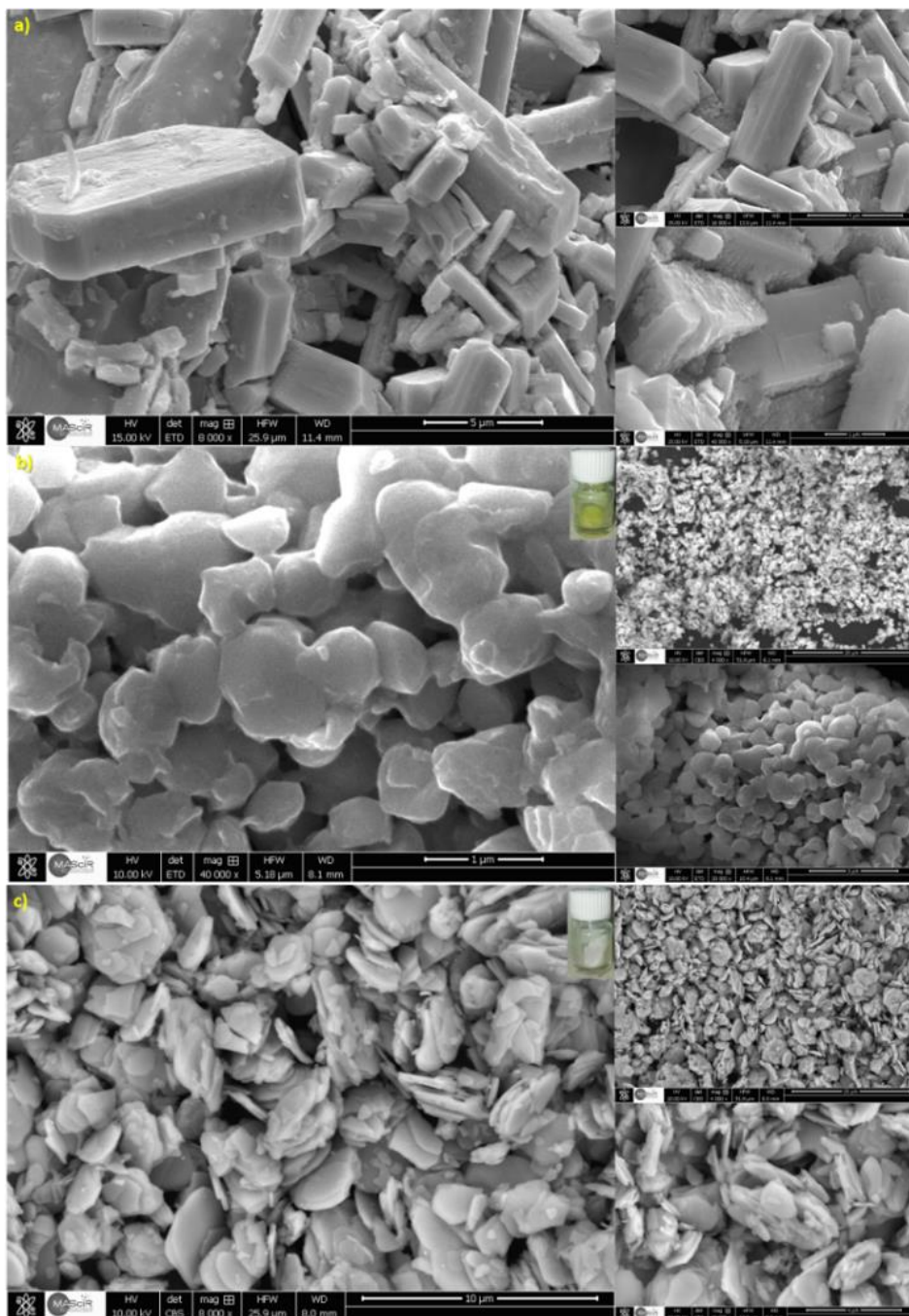
194

**Figure 3.** XRD patterns of (a) compound 1 and 2 and (b) TGA residues.

195 The morphology and microstructure of W10, compound 1 and 2 was investigated by scanning  
 196 Electronic Microscopy (SEM). Figure 4.a shows images of W10, which is constituted by  
 197 parallelepiped crystals of different sizes, the biggest ones having a 11×3×2.84 μm size. These  
 198 parallelepiped crystals resulted from the aggregation of smaller building blocks of about 3.5×1  
 199 μm size.

200 The insertion of CTAB into the structure leads to morphological changes attested by the  
 201 presence of edge-like aggregate with range size of 760-940 nm (Fig.4.b). With a higher  
 202 concentration of CTAB (Fig.4.c), the structure is characterized by the discrete grains of layer  
 203 particles with size in the range 6.61 to 8.5 μm. These observations suggest that the size and the  
 204 morphology of the hybrid materials are different from W10, which indicates, that the use of  
 205 CTAB molecules as a heterogenization agent give rise to a complete change in the morphology  
 206 state of the hybrid materials. In fact, the shape and grain size of hybrid materials changed when  
 207 the CTAB concentration was varied using water as reaction solvent. For compound 1, as the  
 208 concentration of CTAB was close to the critical micelle concentration (CMC = 0,9 mmol in  
 209 water), only a low amount of spherical CTAB micelles were formed leading to small size  
 210 aggregates. On the contrary, with a 4 mM CTAB concentration, much more CTAB micelles are

211 formed and lead to lamellar phases. The aggregation reached 6.84  $\mu\text{m}$ , with a distinct layered  
212 appearance. That indicates the formation of lamellar system which agrees with other study [55].  
213

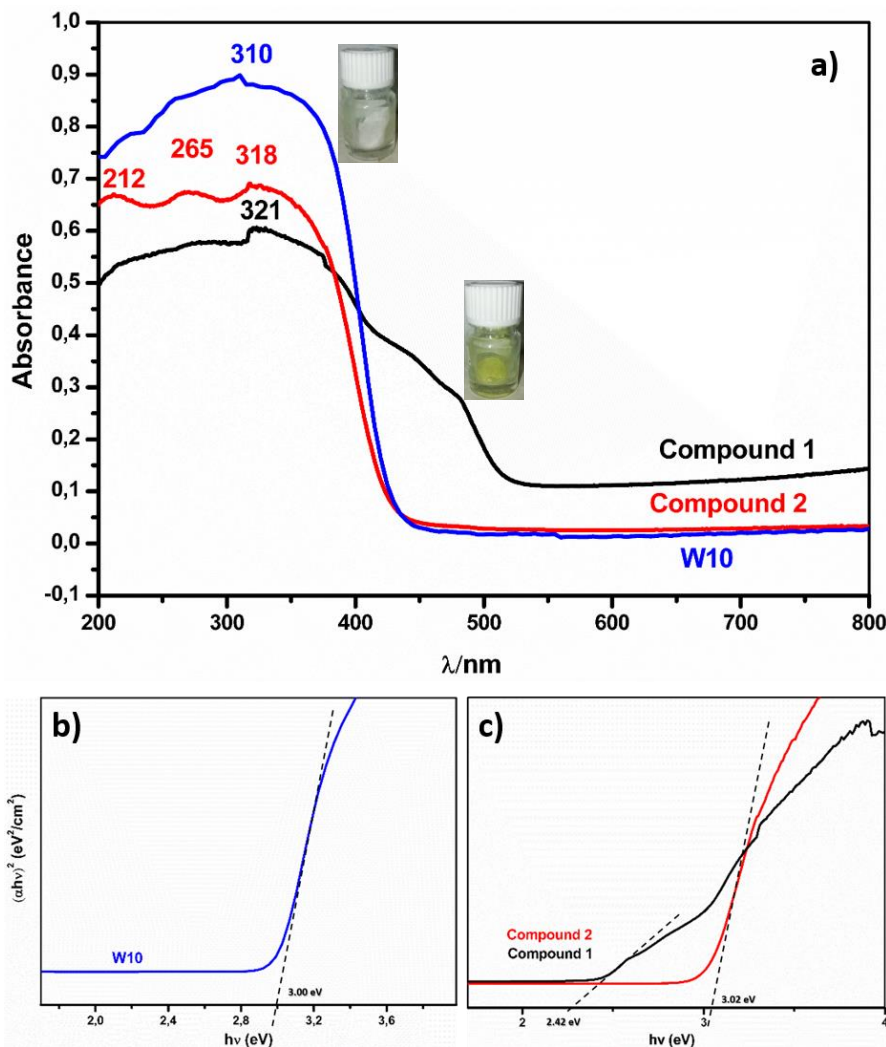


214  
215 **Figure 4** SEM images of W10 (a), compound 1(b) and 2(c).

216 To understand the colour difference (green vs white) between the two hybrid compounds, their  
217 optical properties were investigated.

218 The UV-visible absorption spectra of W10, compound 1 and 2, presented on figure 5.a., show  
219 a large absorption band in UV region. The maximum of absorption is located at 310 and 318

220 nm for W10 and compound **2**, respectively while for compound **1**, this band broadens in the  
 221 visible region until 520 nm. The observed bands for the three compounds are typical to  
 222 decatungstate [46] and are coming from HOMO-LUMO Transition Ligand to Metal Charge  
 223 Transfer (LMCT) and more precisely to the bridging oxygen-to-tungsten charge transfer [56].



224  
 225 **Figure 5.** a) UV-Vis absorption spectra of W10, Compound 1 and 2. b) and c) K-M function  
 226 vs energy (eV).

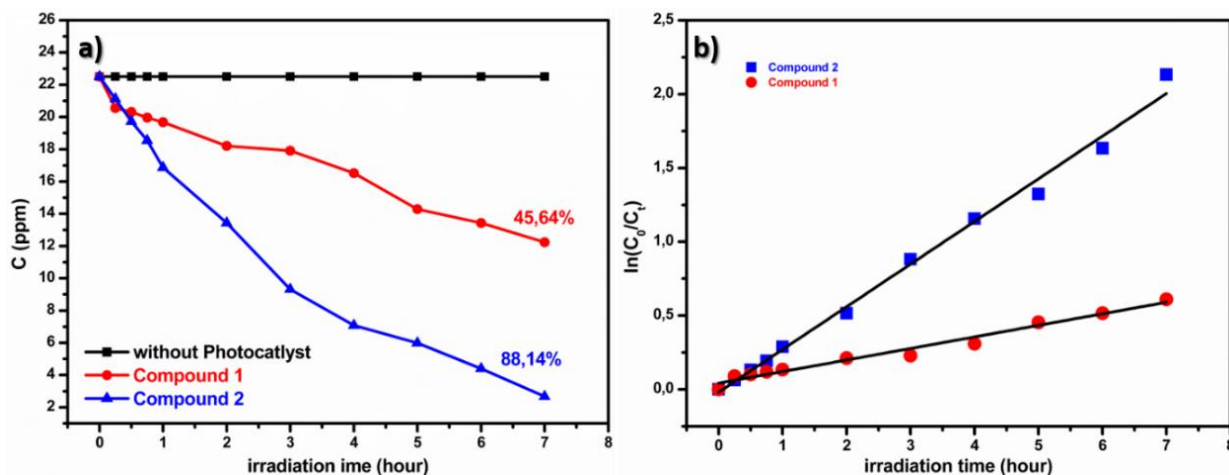
227 To estimate the optical band gap energy  $E_g$ (eV), UV-Visible spectrum was converted to  
 228 Kubelka-Munk function  $\alpha hv = A(hv - E_g)^{n/2}$  and plotted against energy in eV (figure 5.b and 5.c),  
 229 where  $\alpha$  is the absorption coefficient,  $v$  is the light frequency.  $A$  is a constant and  $n$  is the  
 230 transition nature characteristic, which is estimated as a direct transition ( $n=1$ ). The band gap  
 231 energy  $E_g$  can be defined as the intersection between the energy axis and the linear portion of  
 232 the Kubelka-Munk function plot [19,57]. Thus, the band gap energy is equal to 3 eV for W10,  
 233 2.42 for compound **1** and 3.02 eV for compound **2**. These values suggest the promising optical  
 234 properties of our hybrids for visible-light photocatalysis, especially compound **1**. This

235 demonstrates that the use of CTAB molecules as heterogenization agent allow the previous  
236 change in the morphology but also the modification of the optical gap energy.

237

## 238 2.2. Photocatalytic Study

239 In order to evaluate the photocatalytic activities of compound **1** and **2**, a solution of CBZ ( $1 \times 10^{-4}$   
240 mol L<sup>-1</sup>) was irradiated by UV-visible light from 300 W Xe Lamp in the absence and presence  
241 of the photocatalysts. It is worth noting that no direct photodegradation of CBZ is observed as  
242 shown in figure 6.a. On the other hand, in the presence of photocatalysts (30 mg), the  
243 degradation of CBZ were 45.65 and 88.14% after 7 hours of irradiation for compound **1** and **2**  
244 respectively (figure 6.a). The kinetics of CBZ photodegradation by compound **1** and **2** fit with  
245 pseudo-first-order equation as presented in figure 6.b. The apparent kinetic constants ( $k_{app}$ ) of  
246 **1** and **2** under UV-Visible light irradiation are  $7.83 \times 10^{-2}$  and  $2.89 \times 10^{-1} \text{ h}^{-1}$  respectively. The result  
247 indicates that despite the small optical gap energy of compound **1**, its efficiency was lower than  
248 compound **2** as observed previously by Zhao et al. for other hybrid polyoxometalates [58]. In  
249 fact, as the band gap of compound **1** is narrower than that of compound **2**, this is less favourable  
250 to charge separation [58]. Consequently, the production of free hydroxyl radicals is reduced  
251 and the induced photodegradation of organic compounds is decreased [59].

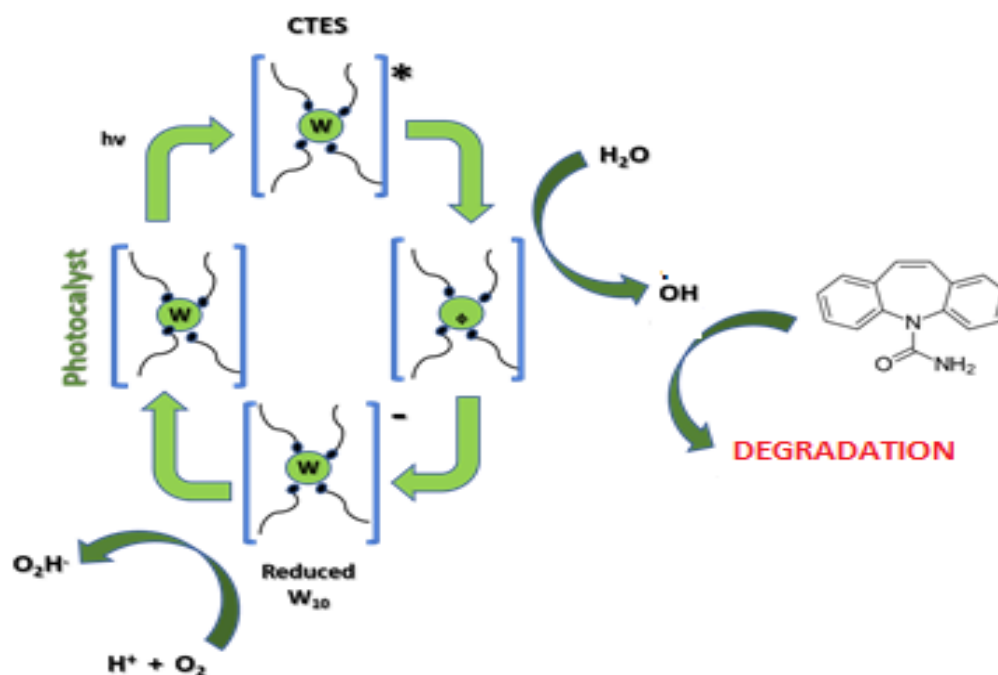


252

253 **Figure 3:** a) Concentration evolution of CBZ under UV irradiation without photocatalyst and  
254 with compound **1** and **2**. b) Kinetics equation of CBZ photodegradation by  
255 compound **1** and **2**.  
256

257 The hydroxyl radicals could be formed as follows: after absorption of photons, decatungstate is  
258 excited with the formation of a charge transfer excited-state ( $W_{10}O_4^{4-}$ )\*, which decays to a very  
259 reactive non-emissive transient species [60]. This species oxidizes water molecules to form

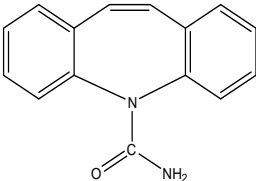
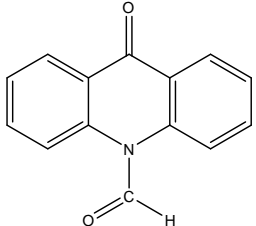
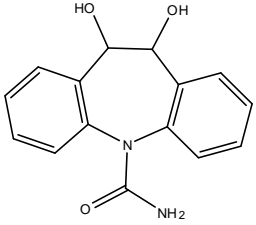
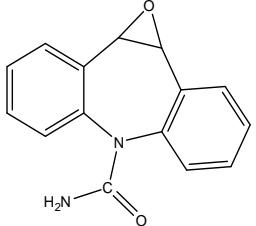
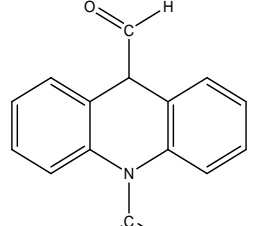
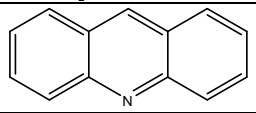
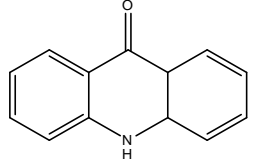
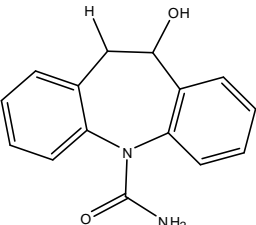
260 hydroxyl radicals ( $\bullet\text{OH}$ ) and a reduced decatungstate [61]. The reduced decatungstate being re-  
 261 oxidized by  $\text{O}_2$  to form again decatungstate and peroxy radicals ( $\text{HO}_2\bullet$ ). This cycle is illustrated  
 262 on figure 7, takes place continuously as long as the system is aerated and exposed to light. The  
 263 formed free radicals, especially  $\bullet\text{OH}$ , can degrade and mineralize CBZ its intermediates  
 264 following a well-known pathway [62–65]. Because of the good efficiency of compound 2, we  
 265 have chosen its kinetics to elucidate carbamazepine degradation pathway; table 1 lists possible  
 266 structures of identified degradation products and their empirical formula and figure 8 illustrate  
 267 the mechanism of photodegradation. According to radicals formation mechanism; ( $\bullet\text{OH}$ ) and  
 268  $\bullet\text{HO}_2$  are the majority radicals present on solution, and are responsible of the degradation of  
 269 carbamazepine and the formation of photoproducts (Figure 8). Indeed, and as a result of  
 270 hydroxylation of CBZ an early-stage products P3 and P4 were observed, P3 in its turn gives  
 271 birth to P7 by epoxy bond cleavage. Thereafter, another hydroxylation takes place to give P2.  
 272 While the loss of  $-\text{COH}$  and  $-\text{NH}_2$  from P4 structure give birth of P1 and P5 [62]. Another  
 273 pathway could be proposed for P4 from P3 via rearrangement [62]. Thereafter, hydroxylation  
 274 of P5 give P6 as a stable product [62,66].



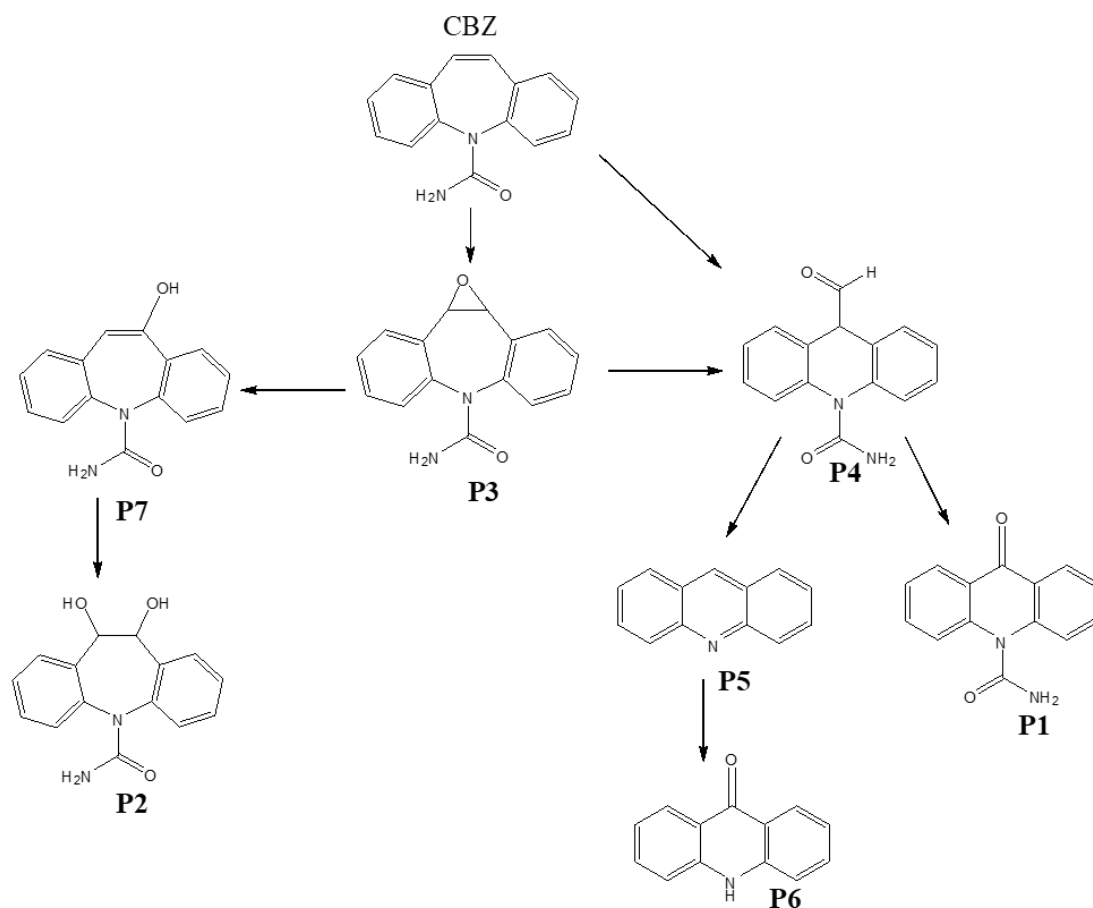
275  
 276 **Figure 4.** Proposed formation mechanism of free hydroxyl radicals by  $(\text{CTA})_4\text{W}_{10}\text{O}_{32}$ .

277  
 278  
 279

**Table 1:** Possible structures of identified degradation products and their empirical formula.

Compound	Retention time (min)	[M+H] <sup>+</sup> m/z	Formula	Proposed structure	Ref
CBZ	4.3	237.1025	C <sub>15</sub> H <sub>12</sub> N <sub>2</sub> O		
P1	1.2	224.0706	C <sub>14</sub> H <sub>9</sub> NO <sub>2</sub>		[41]
P2	2.8	271.1077	C <sub>15</sub> H <sub>14</sub> N <sub>2</sub> O <sub>3</sub>		[41,66,67]
P3	3.06	253.098	C <sub>15</sub> H <sub>12</sub> N <sub>2</sub> O <sub>2</sub>		[67,68]
P4	3.4	253.098	C <sub>15</sub> H <sub>12</sub> N <sub>2</sub> O <sub>2</sub>		[68]
P5	3.4	180.0807	C <sub>13</sub> H <sub>9</sub> N		[41]
P6	3.6	196.0762	C <sub>13</sub> H <sub>9</sub> NO		[41]
P7	4.1	253.098	C <sub>15</sub> H <sub>12</sub> N <sub>2</sub> O <sub>2</sub>		[66,67,69,70]



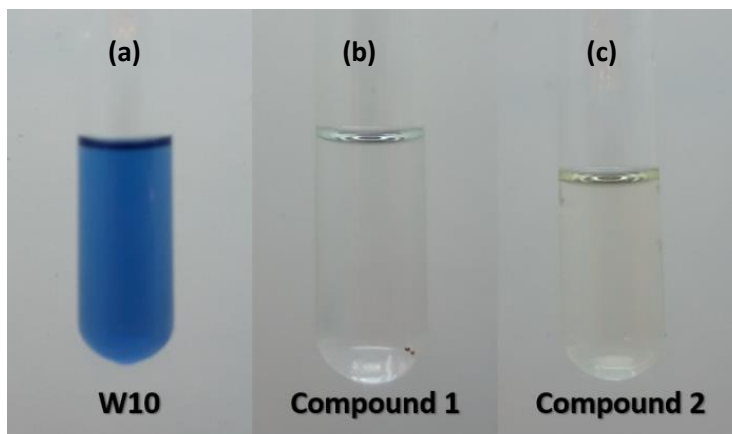


282

283 **Figure 8:** Carbamazepine photo-degradation pathway over compound 2 photo-catalyst.

284 **Leaching Test**

285 The leaching of decatungstate is one of the major drawbacks, which limits the application of  
 286 the hybrid POM materials. To evidence this process, a simple test was carried out at the end of  
 287 each photocatalytic experiment. The photocatalyst was filtered from the solution and a drop of  
 288 ethanol was added to the filtrate and then exposed to UV light. It is well-known that in presence  
 289 of ethanol and under irradiation, anionic decatungstate ( $W_{10}O_{32}^{4-}$ ) is transformed into reduced  
 290 decatungstate ( $W_{10}O_{32}^{5-}$ ) characterized by a blue colour as shown for W10 on figure 9 (a). This  
 291 test allows us to study qualitatively the presence of anionic decatungstate in solution after  
 292 photocatalytic experiment. In figure 9 (b and c) , the absence of a blue colour proved the  
 293 excellent stability of compounds **1** and **2**.



294

295 **Figure 9.** Leaching Tests: In leaching case, the filtrate colour must be change to blue  
296 indicating characteristic of  $W_{10}O_{32}^{5-}$

### 297 **Conclusion**

298 In this study water-insoluble decatungstate based hybrid materials were synthesised in aqueous  
299 media by the reaction of decatungstate anion and a hexadecyltrimethylammonium surfactant  
300 (CTAB) using different molar ratio (1:1 for compound **1** and 1:3 for compound **2**). TGA and  
301 FT-IR spectroscopy reveals the similar elemental composition of both compounds. UV-Visible  
302 spectroscopy and SEM shows the different band gap energy (2.42 eV for **1** and 3.02 eV for **2**)  
303 and the morphology. These materials are used as a photocatalysts for carbamazepine  
304 degradation under UV-visible light irradiation. Both compounds exhibit an interesting  
305 photocatalytic activity especially compound **2** and an excellent chemical stability. Using  
306 surfactant as heterogenization agent for polyoxometalate appears to be a promising strategy for  
307 heterogeneous photocatalysis application.

308

309

310

311

312

313

314

315



316 **References:**

- 317 [1] Y. Guo, C. Hu, Heterogeneous photocatalysis by solid polyoxometalates, (2007) 13.  
318 [http://files/47/Guo et Hu - 2007 - Heterogeneous photocatalysis by solid](http://files/47/Guo%20et%20Hu%20-%20Heterogeneous%20photocatalysis%20by%20solid%20polyoxometal.pdf)  
319 [polyoxometal.pdf](http://files/47/Guo%20et%20Hu%20-%20Heterogeneous%20photocatalysis%20by%20solid%20polyoxometal.pdf).
- 320 [2] C.L. Hill, Progress and challenges in polyoxometalate-based catalysis and catalytic  
321 materials chemistry, (2007) 5. [http://files/44/Hill - 2007 - Progress and challenges in](http://files/44/Hill%20-%20Progress%20and%20challenges%20in%20polyoxometalate-based%20c.pdf)  
322 [polyoxometalate-based c.pdf](http://files/44/Hill%20-%20Progress%20and%20challenges%20in%20polyoxometalate-based%20c.pdf).
- 323 [3] R. Sivakumar, Polyoxometalate-based molecular/nano composites: Advances in  
324 environmental remediation by photocatalysis and biomimetic approaches to solar  
325 energy conversion, (2012) 22. [http://files/46/Sivakumar - 2012 - Polyoxometalate-](http://files/46/Sivakumar%20-%20Polyoxometalate-based%20molecularnano%20composites%20A.pdf)  
326 [based molecularnano composites A.pdf](http://files/46/Sivakumar%20-%20Polyoxometalate-based%20molecularnano%20composites%20A.pdf).
- 327 [4] C. Streb, New trends in polyoxometalate photoredox chemistry: From  
328 photosensitisation to water oxidation catalysis, (2012) 9. [http://files/45/Streb - 2012 -](http://files/45/Streb%20-%20New%20trends%20in%20polyoxometalate%20photoredox%20chemistry.pdf)  
329 [New trends in polyoxometalate photoredox chemistry.pdf](http://files/45/Streb%20-%20New%20trends%20in%20polyoxometalate%20photoredox%20chemistry.pdf).
- 330 [5] S.-S. Wang, G.-Y. Yang, Recent Advances in Polyoxometalate-Catalyzed Reactions,  
331 Chem. Rev. (n.d.) 70. [http://files/48/Wang et Yang - Recent Advances in](http://files/48/Wang%20et%20Yang%20-%20Recent%20Advances%20in%20Polyoxometalate-Catalyzed%20React.pdf)  
332 [Polyoxometalate-Catalyzed React.pdf](http://files/48/Wang%20et%20Yang%20-%20Recent%20Advances%20in%20Polyoxometalate-Catalyzed%20React.pdf).
- 333 [6] Y. Zhou, Z. Guo, W. Hou, Q. Wang, J. Wang, Polyoxometalate-based phase transfer  
334 catalysis for liquid-solid organic reactions: a review, (n.d.) 13. [http://files/43/Zhou et](http://files/43/Zhou%20et%20al.%20-%20Polyoxometalate-based%20phase%20transfer%20catalysis%20for.pdf)  
335 [al. - Polyoxometalate-based phase transfer catalysis for.pdf](http://files/43/Zhou%20et%20al.%20-%20Polyoxometalate-based%20phase%20transfer%20catalysis%20for.pdf).
- 336 [7] A. Bijelic, M. Aureliano, A. Rompel, The antibacterial activity of polyoxometalates:  
337 Structures, antibiotic effects and future perspectives, Chem. Commun. 54 (2018) 1153–  
338 1169. <https://doi.org/10.1039/c7cc07549a>.
- 339 [8] J.T. Rhule, C.L. Hill, D.A. Judd, R.F. Schinazi, Polyoxometalates in Medicine, (n.d.)  
340 32. [http://files/50/Rhule et al. - Polyoxometalates in Medicine.pdf](http://files/50/Rhule%20et%20al.%20-%20Polyoxometalates%20in%20Medicine.pdf).
- 341 [9] M.T. Pope, A. Müller, Polyoxometalate Chemistry: An Old Field with New  
342 Dimensions in Several Disciplines, Angew. Chemie Int. Ed. English. 30 (1991) 34–48.  
343 <https://doi.org/10.1002/anie.199100341>.
- 344 [10] E. Sousa Da Silva, M. Sarakha, H.D. Burrows, P. Wong-Wah-Chung, Decatungstate  
345 anion as an efficient photocatalytic species for the transformation of the pesticide 2-(1-

- 346 naphthyl)acetamide in aqueous solution, *J. Photochem. Photobiol. A Chem.* 334 (2017)  
347 61–73. <https://doi.org/10.1016/j.jphotochem.2016.10.036>.
- 348 [11] V.I. Supranovich, V. V Levin, A.D. Dilman, Radical Addition to N-Tosylimines via C–  
349 H Activation Induced by Decatungstate Photocatalyst, *Org. Lett.* (2019) 4.  
350 [http://files/53/Supranovich et al. - 2019 - Radical Addition to N-Tosylimines via C–H](http://files/53/Supranovich et al. - 2019 - Radical Addition to N-Tosylimines via C–H Activati.pdf)  
351 [Activati.pdf](http://files/53/Supranovich et al. - 2019 - Radical Addition to N-Tosylimines via C–H Activati.pdf).
- 352 [12] C. Tanielian, Decatungstate photocatalyzed oxygenation of methanol in acetonitrile  
353 under photostationary state conditions, (2014) 7.  
354 <http://files/210/10.1016@j.jallcom.2020.155669.pdf>.
- 355 [13] A. Allaoui, M.A. Malouki, P. Wong-Wah-Chung, Homogeneous photodegradation  
356 study of 2-mercaptobenzothiazole photocatalysed by sodium decatungstate salts:  
357 Kinetics and mechanistic pathways, *J. Photochem. Photobiol. A Chem.* 212 (2010)  
358 153–160. <https://doi.org/10.1016/j.jphotochem.2010.04.010>.
- 359 [14] S. Rafqah, P.W.W. Chung, C. Forano, M. Sarakha, Photocatalytic degradation of  
360 metsulfuron methyl in aqueous solution by decatungstate anions, *J. Photochem.*  
361 *Photobiol. A Chem.* 199 (2008) 297–302.  
362 <https://doi.org/10.1016/j.jphotochem.2008.06.012>.
- 363 [15] I. Texier, C. Giannotti, S. Malato, C. Richter, J. Delaire, Solar photodegradation of  
364 pesticides in water by sodium decatungstate, *Catal. Today.* (1999) 11.  
365 [http://files/57/Texier et al. - 1999 - Solar photodegradation of pesticides in water by](http://files/57/Texier et al. - 1999 - Solar photodegradation of pesticides in water by s.pdf)  
366 [s.pdf](http://files/57/Texier et al. - 1999 - Solar photodegradation of pesticides in water by s.pdf).
- 367 [16] B. Orel, U. Lavrenčič-Štangar, M.G. Hutchins, K. Kalcher, Mixed phosphotungstic  
368 acid/titanium oxide gels and thin solid xerogel films with electrochromic-ionic  
369 conductive properties, *J. Non. Cryst. Solids.* 175 (1994) 251–262.  
370 [https://doi.org/10.1016/0022-3093\(94\)90018-3](https://doi.org/10.1016/0022-3093(94)90018-3).
- 371 [17] M.C. Pham, M. Mostefai, P.C. Lacaze, Synthesis and characterization of electrodes  
372 modified by poly(1-naphthol) films doped with heteropolyanions, *Synth. Met.* 52  
373 (1992) 305–317. [https://doi.org/10.1016/0379-6779\(92\)90030-M](https://doi.org/10.1016/0379-6779(92)90030-M).
- 374 [18] S. V. Lomakina, T.S. Shatova, L.P. Kazansky, Heteropoly anions as corrosion  
375 inhibitors for aluminium in high temperature water, *Corros. Sci.* 36 (1994) 1645–1651.  
376 [https://doi.org/10.1016/0010-938X\(94\)90059-0](https://doi.org/10.1016/0010-938X(94)90059-0).

- 377 [19] O. Oulhakem, H. Zahdi, M. Belaïche, S. Laalioui, Z. Naimi, B. Ikken, K.B. Alaoui, Z.  
378 Sekkat, One-step immobilization of tungsten oxide on microporous silica surface as a  
379 photocatalyst for water pollutant removal, *Microporous Mesoporous Mater.* 335 (2022)  
380 111784. <https://doi.org/10.1016/j.micromeso.2022.111784>.
- 381 [20] I. Texier, J.A. Delaire, C. Giannotti, Reactivity of the charge transfer excited state of  
382 sodium decatungstate at the nanosecond time scale, *Phys. Chem. Chem. Phys.* 2 (2000)  
383 1205–1212. <https://doi.org/10.1039/a908588b>.
- 384 [21] F. Bigi, A. Corradini, C. Quarantelli, G. Sartori, Silica-bound decatungstates as  
385 heterogeneous catalysts for H<sub>2</sub>O<sub>2</sub> activation in selective sulfide oxidation, *J. Catal.* 250  
386 (2007) 222–230. <https://doi.org/10.1016/j.jcat.2007.06.019>.
- 387 [22] A. Maldotti, A. Molinari, G. Varani, M. Lenarda, L. Storaro, F. Bigi, R. Maggi, A.  
388 Mazzacani, G. Sartori, Immobilization of (n-Bu<sub>4</sub>N)<sub>4</sub>W<sub>10</sub>O<sub>32</sub> on Mesoporous MCM-  
389 41 and Amorphous Silicas for Photocatalytic Oxidation of Cycloalkanes with  
390 Molecular Oxygen, *J. Catal.* 209 (2002) 210–216.  
391 <https://doi.org/10.1006/jcat.2002.3618>.
- 392 [23] A. Molinari, A. Maldotti, A. Bratovcic, G. Magnacca, Photocatalytic properties of  
393 sodium decatungstate supported on sol–gel silica in the oxidation of glycerol, *Catal.*  
394 *Today.* 206 (2013) 46–52. <https://doi.org/10.1016/j.cattod.2011.11.033>.
- 395 [24] A. Molinari, A. Bratovcic, G. Magnacca, A. Maldotti, Matrix effects on the  
396 photocatalytic oxidation of alcohols by [nBu<sub>4</sub>N]<sub>4</sub>W<sub>10</sub>O<sub>32</sub> incorporated into sol–gel  
397 silica, *Dalt. Trans.* 39 (2010) 7826. <https://doi.org/10.1039/c003282d>.
- 398 [25] A. Molinari, R. Amadelli, A. Mazzacani, G. Sartori, A. Maldotti, Tetralkylammonium  
399 and Sodium Decatungstate Heterogenized on Silica: Effects of the Nature of Cations on  
400 the Photocatalytic Oxidation of Organic Substrates, (n.d.) 6. [http://files/62/Molinari et  
401 al. - Tetralkylammonium and Sodium Decatungstate Heterog.pdf](http://files/62/Molinari%20et%20al.%20-%20Tetralkylammonium%20and%20Sodium%20Decatungstate%20Heterog.pdf).
- 402 [26] S. Farhadi, Z. Momeni, Zirconia-supported sodium decatungstate (Na<sub>4</sub>W<sub>10</sub>O<sub>32</sub>/ZrO<sub>2</sub>):  
403 An efficient, green and recyclable photocatalyst for selective oxidation of activated  
404 alcohols to carbonyl compounds with O<sub>2</sub>, *J. Mol. Catal. A Chem.* 277 (2007) 47–52.  
405 <https://doi.org/10.1016/j.molcata.2007.07.024>.
- 406 [27] S. Farhadi, S. Sepahvand, Na<sub>4</sub>W<sub>10</sub>O<sub>32</sub>/ZrO<sub>2</sub> nanocomposite prepared via a sol-gel  
407 route: A novel, green and recoverable photocatalyst for reductive cleavage of

- 408 azobenzenes to amines with 2-propanol, *J. Mol. Catal. A Chem.* 318 (2010) 75–84.  
409 <https://doi.org/10.1016/j.molcata.2009.11.010>.
- 410 [28] L. Li, Y. Yang, R. Fan, J. Liu, Y. Jiang, B. Yang, W. Cao, Decatungstate acid improves  
411 the photo-induced electron lifetime and retards the recombination in dye sensitized  
412 solar cells, *Dalt. Trans.* 45 (2016) 14940–14947. <https://doi.org/10.1039/C6DT02584F>.
- 413 [29] M.D. Tzirakis, I.N. Lykakis, G.D. Panagiotou, K. Bourikas, A. Lycourghiotis, C.  
414 Kordulis, M. Orfanopoulos, Decatungstate catalyst supported on silica and  $\gamma$ -alumina:  
415 Efficient photocatalytic oxidation of benzyl alcohols, *J. Catal.* (2007) 12.  
416 [http://files/65/Tzirakis et al. - 2007 - Decatungstate catalyst supported on silica and  \$\gamma\$  -  
417 .pdf](http://files/65/Tzirakis et al. - 2007 - Decatungstate catalyst supported on silica and \gamma - .pdf).
- 418 [30] X. Yang, F. Qian, Y. Wang, M. Li, J. Lu, Y. Li, M. Bao, Constructing a novel ternary  
419 composite (C<sub>16</sub>H<sub>33</sub>(CH<sub>3</sub>)<sub>3</sub>N)<sub>4</sub>W<sub>10</sub>O<sub>32</sub>/g-C<sub>3</sub>N<sub>4</sub>/rGO with enhanced visible-light-  
420 driven photocatalytic activity for degradation of dyes and phenol, *Appl. Catal. B*  
421 *Environ.* 200 (2017) 283–296. <https://doi.org/10.1016/j.apcatb.2016.07.024>.
- 422 [31] A. Misra, K. Kozma, C. Streb, M. Nyman, Beyond Charge Balance: Counter-Cations  
423 in Polyoxometalate Chemistry, *Angew. Chemie - Int. Ed.* 59 (2020) 596–612.  
424 <https://doi.org/10.1002/anie.201905600>.
- 425 [32] T. Ito, T. Yamase, Controllable Layered Structures in Polyoxomolybdate-Surfactant  
426 Hybrid Crystals, *Materials (Basel)*. 3 (2010) 158–164.  
427 <https://doi.org/10.3390/ma3010158>.
- 428 [33] M. Nyman, M.A. Rodriguez, T.M. Anderson, D. Ingersoll, Two Structures Toward  
429 Understanding Evolution from Surfactant-Polyoxometalate Lamellae to Surfactant-  
430 Encapsulated Polyoxometalates, *Cryst. Growth Des.* 9 (2009) 3590–3597.  
431 <https://doi.org/10.1021/cg9003356>.
- 432 [34] M. Nyman, D. Ingersoll, S. Singh, F. Bonhomme, T.M. Alam, C.J. Brinker, M.A.  
433 Rodriguez, Comparative Study of Inorganic Cluster-Surfactant Arrays, (n.d.) 11.  
434 <http://files/19/Nyman et al. - Comparative Study of Inorganic Cluster-Surfactant .pdf>.
- 435 [35] B. Ohtani, Preparing Articles on Photocatalysis—Beyond the Illusions,  
436 Misconceptions, and Speculation, *Chem. Lett.* 37 (2008) 216–229.  
437 <https://doi.org/10.1246/cl.2008.216>.

- 438 [36] X. Yan, T. Ohno, K. Nishijima, R. Abe, B. Ohtani, Is methylene blue an appropriate  
439 substrate for a photocatalytic activity test? A study with visible-light responsive titania,  
440 Chem. Phys. Lett. (2006) 5. [http://files/168/\[Pure and Applied Chemistry\]](http://files/168/[Pure and Applied Chemistry])  
441 Physisorption of gases with special reference to the evaluation of surface area and pore  
442 size distribution (IUPAC Technical Report).pdf.
- 443 [37] R. Andreozzi, M. Raffaele, Pharmaceuticals in STP effluents and their solar  
444 photodegradation in aquatic environment, (2003) 12. <http://files/15/Andreozzi et>  
445 Raffaele - 2003 - Pharmaceuticals in STP effluents and their solar pho.pdf.
- 446 [38] P. Falås, H.R. Andersen, A. Ledin, Occurrence and reduction of pharmaceuticals in the  
447 water phase at Swedish wastewater treatment plants, Water Sci. (2012) 10.  
448 <http://files/13/Falås et al. - 2012 - Occurrence and reduction of pharmaceuticals in>  
449 the.pdf.
- 450 [39] C.D. Metcalfe, X.-S. Miao, B.G. Koenig, J. Struger, Distribution of acidic and neutral  
451 drugs in surface waters near sewage treatment plants in the lower Great Lakes, Canada,  
452 (n.d.) 9. <http://files/14/Metcalfe et al. - Distribution of acidic and neutral drugs in>  
453 surfac.pdf.
- 454 [40] P.E. Stackelberg, J. Gibs, E.T. Furlong, M.T. Meyer, S.D. Zaugg, R.L. Lippincott,  
455 Efficiency of conventional drinking-water-treatment processes in removal of  
456 pharmaceuticals and other organic compounds, Sci. Total Environ. (2007) 18.  
457 <http://files/198/duan2019.pdf>.
- 458 [41] R. Meribout, Y. Zuo, A.A. Khodja, A. Piram, S. Lebarillier, J. Cheng, C. Wang, P.  
459 Wong-Wah-Chung, Photocatalytic degradation of antiepileptic drug carbamazepine  
460 with bismuth oxychlorides (BiOCl and BiOCl/AgCl composite) in water: Efficiency  
461 evaluation and elucidation degradation pathways, J. Photochem. Photobiol. A Chem.  
462 328 (2016) 105–113. <https://doi.org/10.1016/j.jphotochem.2016.04.024>.
- 463 [42] O.Y. Poimanova, S. V Radio, K.Y. Bilousova, V.N. Baumer, G.M. Rozantsev,  
464 Equilibria in the acidified aqueous-dimethylformamide solutions of tungstate-anion.  
465 Synthesis, crystal structure and characterization of decatungstate, (n.d.) 33.  
466 <http://files/25/Poimanova et al. - Equilibria in the acidified aqueous->  
467 dimethylformam.pdf.
- 468 [43] O.Y. Poimanova, S. V Radio, K.Y. Bilousova, D. V Khaustov, V.N. Baumer, G.M.

- 469 Rozantsev, Phase formation in the system  $\text{Co}^{2+} - \text{WO}_4^{2-} - \text{H}^+ - \text{C}_3\text{H}_7\text{ON} - \text{H}_2\text{O}$ .  
470 Synthesis, crystal structure and characterization of cobalt(II) decatungstate, (n.d.) 25.  
471 [http://files/26/Poimanova et al. - Phase formation in the system  \$\text{Co}^{2+} - \text{WO}\_4^{2-} - \text{H}^+ -\$](http://files/26/Poimanova et al. - Phase formation in the system Co2+ - WO42- - H+ - .pdf)   
472 [.pdf](#).
- 473 [44] R.B. Viana, Infrared Spectroscopy of Anionic, Cationic, and Zwitterionic Surfactants,  
474 *Adv. Phys. Chem.* (n.d.) 15. [http://files/27/Viana - Infrared Spectroscopy of Anionic,](http://files/27/Viana - Infrared Spectroscopy of Anionic, Cationic, and Zw.pdf)  
475 [Cationic, and Zw.pdf](#).
- 476 [45] V. Kulikov, G. Meyer, Organoamine silver(I) decatungstate structures: remarkable  
477 chemoselectivity and the exploration of the intramolecular redox reaction upon  
478 thermolysis, *New J. Chem.* 38 (2014) 3408. <https://doi.org/10.1039/C4NJ00172A>.
- 479 [46] S. Wang, S. Xing, Z. Shi, J. He, Q. Han, M. Li, Electrostatic polypyridine–ruthenium(  
480 II)···decatungstate dyads: structures, characterizations and photodegradation of dye,  
481 *RSC Adv.* 7 (2017) 18024–18031. <https://doi.org/10.1039/C7RA01342F>.
- 482 [47] V. Kulikov, G. Meyer, Polyoxotungstates in Molecular Boxes of Purine Bases, (2014)  
483 10. [http://files/23/Kulikov et Meyer - 2014 - Polyoxotungstates in Molecular Boxes of](http://files/23/Kulikov et Meyer - 2014 - Polyoxotungstates in Molecular Boxes of Purine Bas.pdf)  
484 [Purine Bas.pdf](#).
- 485 [48] M. Avila, L. Reguera, J. Rodríguez-Hernández, J. Balmaseda, E. Reguera, Porous  
486 framework of  $\text{T}_2[\text{Fe}(\text{CN})_6] \cdot x\text{H}_2\text{O}$  with  $\text{T}=\text{Co}, \text{Ni}, \text{Cu}, \text{Zn}$ , and  $\text{H}_2$  storage, *J. Solid*  
487 *State Chem.* 181 (2008) 2899–2907. <https://doi.org/10.1016/j.jssc.2008.07.030>.
- 488 [49] X.H. Liu, X.H. Luo, S.X. Lu, J.C. Zhang, W.L. Cao, A novel cetyltrimethyl  
489 ammonium silver bromide complex and silver bromide nanoparticles obtained by the  
490 surfactant counterion, *J. Colloid Interface Sci.* 307 (2007) 94–100.  
491 <https://doi.org/10.1016/j.jcis.2006.11.051>.
- 492 [50] Z. Sui, X. Chen, L. Wang, Y. Chai, C. Yang, J. Zhao, An improved approach for  
493 synthesis of positively charged silver nanoparticles, *Chem. Lett.* 34 (2005) 100–101.  
494 <https://doi.org/10.1246/cl.2005.100>.
- 495 [51] Z.M. Sui, X. Chen, L.Y. Wang, L.M. Xu, W.C. Zhuang, Y.C. Chai, C.J. Yang,  
496 Capping effect of CTAB on positively charged Ag nanoparticles, *Phys. E Low-*  
497 *Dimensional Syst. Nanostructures.* 33 (2006) 308–314.  
498 <https://doi.org/10.1016/j.physe.2006.03.151>.

- 499 [52] J.M. Salazar, G. Weber, J.M. Simon, I. Bezverkhyy, J.P. Bellat, Characterization of  
500 adsorbed water in MIL-53(Al) by FTIR spectroscopy and ab-initio calculations, *J.*  
501 *Chem. Phys.* 142 (2015). <https://doi.org/10.1063/1.4914903>.
- 502 [53] S.H. Wu, D.H. Chen, Synthesis of high-concentration Cu nanoparticles in aqueous  
503 CTAB solutions, *J. Colloid Interface Sci.* 273 (2004) 165–169.  
504 <https://doi.org/10.1016/j.jcis.2004.01.071>.
- 505 [54] A.T. Shah, A. Mujahid, M.U. Farooq, W. Ahmad, B. Li, M. Irfan, M.A. Qadir, Micelle  
506 directed synthesis of (C<sub>19</sub>H<sub>42</sub>N)<sub>4</sub>H<sub>3</sub>(PW<sub>11</sub>O<sub>39</sub>) nanoparticles and their catalytic  
507 efficiency for oxidative degradation of azo dye, *J. Sol-Gel Sci. Technol.* 63 (2012)  
508 194–199. <https://doi.org/10.1007/s10971-012-2779-6>.
- 509 [55] L. Wei, Z. Ming, Z. Jinli, H. Yongcai, Self-assembly of cetyl trimethylammonium  
510 bromide in ethanol-water mixtures, (n.d.) 5. [http://files/28/Wei et al. - Self-assembly of  
511 cetyl trimethylammonium bromide i.pdf](http://files/28/Wei%20et%20al.%20-%20Self-assembly%20of%20cetyl%20trimethylammonium%20bromide%20i.pdf).
- 512 [56] D. Ravelli, D. Dondi, M. Fagnoni, A. Albini, A. Bagnò, Electronic and EPR spectra of  
513 the species involved in [W<sub>10</sub>O<sub>32</sub>]<sup>4-</sup> photocatalysis. A relativistic DFT investigation,  
514 *Phys. Chem. Chem. Phys.* 15 (2013) 2890. <https://doi.org/10.1039/c2cp43950f>.
- 515 [57] Z. Chen, H.N. Dinh, E. Miller, Photoelectrochemical water splitting: standards,  
516 experimental methods, and protocols, Springer, New York, 2013. [http://files/30/Chen  
517 et al. - 2013 - Photoelectrochemical water splitting standards, e.pdf](http://files/30/Chen%20et%20al.%20-%202013%20-%20Photoelectrochemical%20water%20splitting%20standards,%20e.pdf).
- 518 [58] X. Zhao, S. Zhang, J. Yan, L. Li, G. Wu, W. Shi, G. Yang, N. Guan, P. Cheng,  
519 Polyoxometalate-Based Metal–Organic Frameworks as Visible-Light-Induced  
520 Photocatalysts, *Inorg. Chem.* (2018) 8. [http://files/33/Zhao et al. - 2018 -  
521 Polyoxometalate-Based Metal–Organic Frameworks as .pdf](http://files/33/Zhao%20et%20al.%20-%202018%20-%20Polyoxometalate-Based%20Metal-Organic%20Frameworks%20as%20.pdf).
- 522 [59] J.T. Jasper, D.L. Sedlak, Phototransformation of Wastewater-Derived Trace Organic  
523 Contaminants in Open-Water Unit Process Treatment Wetlands, *Environ. Sci.* (n.d.)  
524 10. [http://files/34/Jasper et Sedlak - Phototransformation of Wastewater-Derived Trace  
525 Or.pdf](http://files/34/Jasper%20et%20Sedlak%20-%20Phototransformation%20of%20Wastewater-Derived%20Trace%20Or.pdf).
- 526 [60] D.C. Duncan, T.L. Netzel, C.L. Hill, Early-Time Dynamics and Reactivity of  
527 Polyoxometalate Excited States. Identification of a Short-Lived LMCT Excited State  
528 and a Reactive Long-Lived Charge-Transfer Intermediate following Picosecond Flash  
529 Excitation of [W<sub>10</sub>O<sub>32</sub>]<sup>4-</sup> in Acetonitrile, *Inorg. Chem.* 34 (1995) 4640–4646.

- 530 <https://doi.org/10.1021/ic00122a021>.
- 531 [61] A. Molinari, R. Argazzi, A. Maldotti, Photocatalysis with Na<sub>4</sub>W<sub>10</sub>O<sub>32</sub> in water  
532 system: Formation and reactivity of OH radicals, *J. Mol. Catal. A Chem.* 372 (2013)  
533 23–28. <https://doi.org/10.1016/j.molcata.2013.01.037>.
- 534 [62] Y. Duan, Assembly of graphene on Ag<sub>3</sub>PO<sub>4</sub>/AgI for effective degradation of  
535 carbamazepine under Visible-light irradiation: Mechanism and degradation pathways,  
536 (n.d.) 37. [http://files/38/Duan - Assembly of graphene on Ag<sub>3</sub>PO<sub>4</sub>AgI for effective](http://files/38/Duan - Assembly of graphene on Ag3PO4AgI for effective)  
537 [d.pdf](#).
- 538 [63] Z. Hu, X. Cai, Z. Wang, S. Li, Z. Wang, X. Xie, Construction of carbon-doped  
539 supramolecule-based g-C<sub>3</sub>N<sub>4</sub>/TiO<sub>2</sub> composites T for removal of diclofenac and  
540 carbamazepine: A comparative study of operating parameters, mechanisms,  
541 degradation pathways, *J. Hazard. Mater.* (2019) 14. <http://files/39/Hu et al. - 2019 ->  
542 [Construction of carbon-doped supramolecule-based g.pdf](#).
- 543 [64] S. Li, Z. Wang, X. Zhao, X. Yang, G. Liang, X. Xie, Insight into enhanced  
544 carbamazepine photodegradation over biochar-based magnetic photocatalyst  
545 Fe<sub>3</sub>O<sub>4</sub>/BiOBr/BC under visible LED light irradiation, *Chem. Eng. J.* 360 (2019) 600–  
546 611. <https://doi.org/10.1016/j.cej.2018.12.002>.
- 547 [65] M. Moztahida, J. Jang, M. Nawaz, S.-R. Lim, D.S. Lee, Effect of rGO loading on  
548 Fe<sub>3</sub>O<sub>4</sub>: A visible light assisted catalyst material for carbamazepine degradation, *Sci.*  
549 *Total Environ.* (2019) 10. <http://files/40/Moztahida et al. - 2019 - Effect of rGO loading>  
550 [on Fe3O4 A visible light as.pdf](#).
- 551 [66] Y. Hong, H. Zhou, Z. Xiong, Y. Liu, G. Yao, B. Lai, Heterogeneous activation of  
552 peroxymonosulfate by CoMgFe-LDO for degradation of carbamazepine: Efficiency,  
553 mechanism and degradation pathways, *Chem. Eng. J.* (2019) 123604.  
554 <https://doi.org/10.1016/j.cej.2019.123604>.
- 555 [67] M. Nawaz, W. Miran, J. Jang, D.S. Lee, One-step hydrothermal synthesis of porous 3D  
556 reduced graphene oxide/TiO<sub>2</sub> aerogel for carbamazepine photodegradation in aqueous  
557 solution, *Appl. Catal. B Environ.* 203 (2017) 85–95.  
558 <https://doi.org/10.1016/j.apcatb.2016.10.007>.
- 559 [68] A.B. Martínez-Piernas, S. Nahim-Granados, M.I. Polo-López, P. Fernández-Ibáñez, S.  
560 Murgolo, G. Mascolo, A. Agüera, Identification of transformation products of



- 561 carbamazepine in lettuce crops irrigated with Ultraviolet-C treated water, Environ.  
562 Pollut. 247 (2019) 1009–1019. <https://doi.org/10.1016/j.envpol.2019.02.001>.
- 563 [69] C. Tanielian, K. Duffy, A. Jones, Kinetic and Mechanistic Aspects of Photocatalysis by  
564 Polyoxotungstates: A Laser Flash Photolysis, Pulse Radiolysis, and Continuous  
565 Photolysis Study, (n.d.) 7. [http://files/41/Tanielian et al. - Kinetic and Mechanistic  
566 Aspects of Photocatalysis .pdf](http://files/41/Tanielian%20et%20al.%20-%20Kinetic%20and%20Mechanistic%20Aspects%20of%20Photocatalysis.pdf).
- 567 [70] V. De Waele, O. Poizat, M. Fagnoni, A. Bagno, D. Ravelli, Unraveling the Key  
568 Features of the Reactive State of Decatungstate Anion in Hydrogen Atom Transfer  
569 (HAT) Photocatalysis, ACS Catal. (2016) 9. [http://files/42/Waele et al. - 2016 -  
570 Unraveling the Key Features of the Reactive State .pdf](http://files/42/Waele%20et%20al.%20-%202016%20-%20Unraveling%20the%20Key%20Features%20of%20the%20Reactive%20State.pdf).

571

572

573

574